JBC RESEARCH ARTICLE

A single amino acid residue tunes the stability of the fully reduced flavin cofactor and photorepair activity in photolyases

Received for publication, May 20, 2022, and in revised form, June 14, 2022 Published, Papers in Press, June 24, 2022,
https://doi.org/10.1016/j.jbc.2022.102188

Bin Wen[1,‡], **Lei Xu**[2,‡], **Yawei Tang**[1], **Zhen Jiang**[1], **Mengting Ge**[1], **Li Liu**[1], **and Guoping Zhu**[1,*]

From the [1]*Anhui Provincial Key Laboratory of Molecular Enzymology and Mechanism of Major Diseases, College of Life Sciences, Anhui Normal University, Wuhu, Anhui, China;* [2]*Anhui Province Key Laboratory of Active Biological Macro-molecules, Wannan Medical College, Wuhu, Anhui, China*

Edited by F. Peter Guengerich

The UV-induced DNA lesions, cyclobutane pyrimidine dimers (CPDs) and pyrimidine (6-4) pyrimidone photoproducts (6-4 photoproducts), can be directly photorepaired by CPD photolyases and 6-4 photolyases, respectively. The fully reduced flavin (hydroquinone, HQ) cofactor is required for the catalysis of both types of these photolyases. On the other hand, flavin cofactor in the semireduced state, semiquinone, can be utilized by photolyase homologs, the cryptochromes. However, the evolutionary process of the transition of the functional states of flavin cofactors in photolyases and cryptochromes remains mysterious. In this work, we investigated three representative photolyases (*Escherichia coli* CPD photolyase, *Microcystis aeruginosa* DASH, and *Phaeodactylum tricornutum* 6-4 photolyase). We show that the residue at a single site adjacent to the flavin cofactor (corresponding to Ala377 in *E. coli* CPD photolyase, hereafter referred to as site 377) can fine-tune the stability of the HQ cofactor. We found that, in the presence of a polar residue (such as Ser or Asn) at site 377, HQ was stabilized against oxidation. Furthermore, this polar residue enhanced the photorepair activity of these photolyases both *in vitro* and *in vivo*. In contrast, substitution of hydrophobic residues, such as Ile, at site 377 in these photolyases adversely affected the stability of HQ. We speculate that these differential residue preferences at site 377 in photolyase proteins might reflect an important evolutionary event that altered the stability of HQ on the timeline from expression of photolyases to that of cryptochromes.

The cryptochrome/photolyase family (CPF) represents a large protein family that is widely distributed in all kingdoms of life (1). Most CPF members contain a flavin adenine dinucleotide (FAD) cofactor, which may be in different redox states, such as fully reduced hydroquinone (HQ, $FADH^-$), neutral semiquinone (SQ) (NSQ, $FADH^\bullet$), anionic SQ (ASQ, $FAD^{\bullet-}$), and fully oxidized (OX) state (2). Photolyases are enzymes that repair UV-induced DNA lesions by using external light energy. There are two major UV-induced DNA lesions, cyclobutane pyrimidine dimers (CPDs) and pyrimidine (6-4) pyrimidone photoproducts (6-4 photoproducts). These lesions can be recognized and repaired by two types of photolyases, named CPD photolyases and 6-4 photolyases, respectively (1, 3). The repair mechanisms of both types of photolyases are similar that require a FAD cofactor in the HQ state. Briefly, a photolyase binds to a segment of DNA containing a lesion at first. Then, the lesion is flipped out of the DNA duplex into the active site of the enzyme to form a stable complex. The energy of one or two photons is directly absorbed by the FAD cofactor in the HQ state or transferred to the cofactor *via* an antenna cofactor to generate excited HQ. The excited HQ donates an electron to the lesion to form a charge-separated radical pair (lesion radical + NSQ). Finally, the lesion radical is split to give two pyrimidines and the excess electron returns to the NSQ to restore the HQ state (3–6). Despite the similarities in the catalytic process, the substrates of these two types of photolyases are not interchangeable. The catalytic quantum yields of 6-4 photolyases (0.05–0.10) are much lower than those of CPD photolyases (0.40–1.00) (3–6). Moreover, some characteristic functional motifs are found only in 6-4 photolyases but not in CPD photolyases, such as the phosphate-binding motif, the Pro-Lys-Leu protrusion motif, and the sulfur loop (7). Recently, a functional conversion study showed that a 6-4 photolyase can be engineered into a CPD photolyase by mutagenesis, but the attempt to convert a CPD photolyase to a 6-4 photolyase was not successful (8). It was proposed that CPD photolyases are ancestors of CPF instead of 6-4 photolyases (9).

Cryptochromes (CRYs) are the proteins that share highly homologous sequences and structures with photolyases but usually lack DNA repair activity (2). Plant CRYs are photoreceptors that regulate the blue light–dependent growth and development of plants, such as inhibition of hypocotyl elongation, stimulation of cotyledon expansion, and promotion of floral initiation (10). Animal CRYs can be divided into several types. Type I animal CRYs (such as *d*CRY in *Drosophila*) are the light-dependent receptors for the entrainment of the circadian rhythm. Type II animal CRYs (*e.g.*, CRY1 and CRY2

‡ These authors contributed equally to this work.
* For correspondence: Guoping Zhu, gpz2012@ahnu.edu.cn.

in mouse and human) are light-independent regulatory components of the circadian clock (2). Type 0 CRYs are found in sponges, which may sense light in the primordial eyes of sponges (11, 12). Type IV animal CRYs are discovered in birds, amphibians, fish, and reptiles, which may act as light-dependent magnetosensors (12–14). Phylogenetic analysis shows that different types of CRYs have diverse evolutionary histories. Plant CRYs are similar to CPD photolyases, whereas animal CRYs are closely related to 6-4 photolyases (2, 12, 15). In contrast to photolyases, plant and animal CRYs do not possess the HQ but the SQ (NSQ for plant CRYs and ASQ for type I animal CRYs) in their possible signaling states (2, 10, 16).

Another type of CRY, named DASH, is found in many prokaryotes and eukaryotes, which has a close relationship to the animal CRYs and 6-4 photolyases (2, 12, 17). However, DASH proteins are highly stable in the HQ state, and some of them have repair activity for CPDs in ssDNA or dsDNA, which should be better categorized as a special class of CPD photolyases (18–24). Due to possessing the possible dual function as DNA repair activity and photoreceptor, DASH proteins may therefore represent an evolutionary intermediate state between photolyases and CRYs (23–26). Nevertheless, a number of 6-4 photolyases, such as *Phaeodactylum tricornutum* 6-4 photolyase (*Pt*CPF1), was shown possessing CRY-like functions, indicating that they are also intermediates between photolyases and CRYs (27–30).

During the evolution process from photolyases to CRYs, the functional states of the FAD cofactor are changed from the HQ to the SQ state. It is intriguing to find out which differences in the structures of photolyases and CRYs are the key reasons for the transition of the functional states of FAD. The most prominent structural differences are found at a site proximal to the N5 of FAD (Asn378 in *Escherichia coli* CPD photolyase [*Ec*CPD], hereafter referred to as site 378). An asparagine (N) residue is conserved in CPD photolyases, 6-4 photolyases and DASH proteins (31–35). In contrast, an aspartic acid (D) and a cysteine (C) were found at site 378 of plant CRYs and type I animal CRYs, respectively. These two residues were considered to be crucial for stabilizing the NSQ and ASQ states in plant CRYs and type I animal CRYs (33, 36–40). However, the mutation researches showed that N378D and N378C mutants of *Ec*CPD did not represent the exact features of corresponding CRYs (33, 34). These results indicate that a single residue change is not enough to convert a photolyase to a CRY, the substitutions of other residues must be necessary.

In our previous work, it was found that the residues at a site that is located above the *si* face of the isoalloxazine ring of the FAD cofactor (Ala377 in *Ec*CPD, site 377) have an interesting distribution pattern in the CPF proteins. Most CPD photolyases and DASH proteins contain small or polar residues such as Ala, Ser, or Asn at this site. Meanwhile, most 6-4 photolyases and animal CRYs contain hydrophobic residues such as Ile, Leu, or Val at this site (41). It was demonstrated that replacing Ala377 in *Ec*CPD with hydrophobic residues impaired the binding affinity for the HQ state FAD. Conversely, the FAD cofactor was photoreduced beyond the ASQ state to the HQ state after extensive illumination in the *d*CRY mutants in which the homologous residue at site 377 (Val415) was mutated to polar residues. These results implicated that the residues at site 377 affect the preferences of the CPF proteins to the HQ state FAD (41). However, there are some shortcomings of our previous work. The observed lower affinity for the HQ state FAD might result from denaturation of the mutant proteins after prolonged red light illumination under aerobic conditions. And we found that a number of 6-4 photolyases with hydrophobic residues at site 377 associate with the HQ state FAD tightly after being photoreduced. Nevertheless, more CPF proteins are needed to verify the exact effect of the residues at site 377. In this study, we focused on site 377 in three representative CPF proteins (*Ec*CPD, *Microcystis aeruginosa* DASH (*Ma*DASH), *Pt*CPF1) to gain deeper insights into the site. Mutants of the three photolyases at site 377 were constructed and investigated. The results revealed that the residues at site 377 have an appreciable impact on the HQ stability against oxidation of these proteins. Based on these findings, we speculated that the different residue preferences at site 377 in CPD photolyases, DASH proteins, 6-4 photolyases, and CRYs may reflect a series of evolutionary events from CPD photolyases to animal CRYs, with DASH proteins and/or 6-4 photolyases as the intermediates.

Results

Sequence and structure analyses of the CPF proteins

Photolyases and CRYs belong to the same protein family named CPF and share many structural features. However, they have diverse functions accompanied with different functional states of their FAD cofactors. Photolyases could repair CPDs or 6-4 photoproducts in DNA only with FAD in the HQ state (3–6). Meanwhile, plant CRYs and type I animal CRYs require the NSQ and ASQ to perform their signaling functions, respectively (2, 10, 16). To elucidate the molecular foundation of these differences between photolyases and CRYs, sequence analyses of the CPF proteins were conducted. The phylogenetic tree showed that the CPF proteins were divided into seven main groups as previously reported: class I CPD photolyases, class III CPD photolyases (including plant CRYs), DASH proteins, 6-4 photolyases (including animal CRYs), class II CPD photolyases, FeS-BCP (iron-sulfur bacterial CRYss and photolyases), and SPL (short photolyase-like) proteins (Fig. 1) (2, 9, 41, 42). Class II CPD photolyases, FeS-BCP, and SPL proteins have low sequence homology to other groups, which formed three separated clusters. In contrast, class I CPD photolyases, class III CPD photolyases (including plant CRYs), DASH proteins, and 6-4 photolyases (including animal CRYs) branched from one node (marked with an asterisk in Fig. 1) in the tree, indicating that they might have a common ancestor. Because class I and class III CPD photolyases are predominantly found in prokaryotes, DASH proteins are found both in prokaryotes and eukaryotes, 6-4 photolyases are dominantly observed in eukaryotes, we

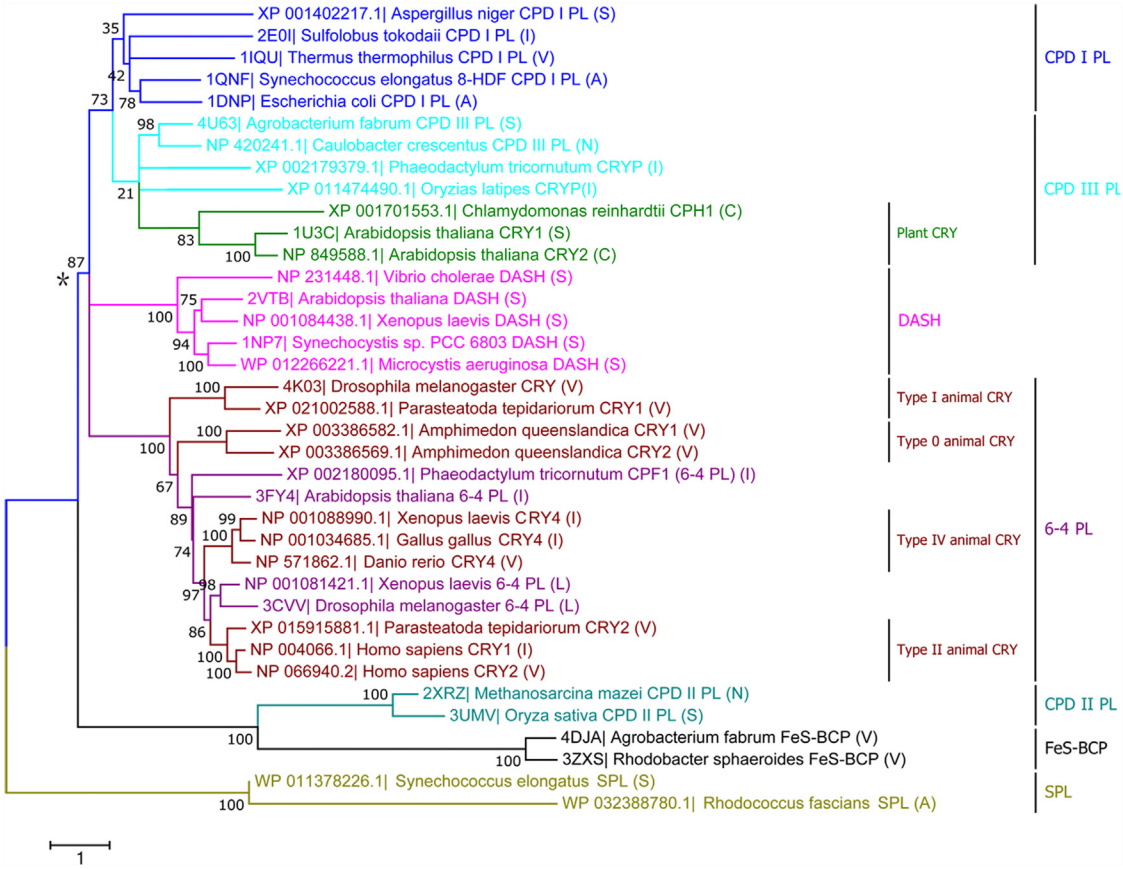

Figure 1. Phylogenetic tree with 37 selected CPF proteins. The evolutionary history was inferred by using the maximum likelihood method and 500 bootstrap iterations. Numbers above nodes represent the bootstrap support percentage values. The CPF proteins were divided into seven main groups: class I CPD photolyases (CPD I PL), class III CPD photolyases (CPD III PL), DASH proteins, 6-4 photolyases (6-4 PL), class II CPD photolyases (CPD III PL), FeS-BCP, and SPL proteins. Plant CRYs, and type 0 to type IV animal CRYs were are clustered as the subgroups of CPD III PL and 6-4 PL, respectively. The node contains CPD I PL, CPD III PL (including plant CRYs), DASH proteins, and 6-4 PL (including animal CRYs) was marker with an asterisk. CPD, cyclobutane pyrimidine dimer.

proposed that the common ancestor at the node should be a protein like a class I/III CPD photolyase. DASH proteins might be intermediates between class I/III CPD photolyases and 6-4 photolyases/animal CRYs. Therefore, a possible evolutionary route from photolyases to animal CRYs was proposed: ancestor like a class I/III CPD photolyase → DASH proteins → 6-4 photolyases → animal CRYs. Nevertheless, another evolutionary route cannot be ruled out, that 6-4 photolyases were directly evolved from an ancestor like a class I/III CPD photolyase, and derived various animal CRYs.

Next, we investigated the structural features of the CPF proteins. Figure 2 shows the aligned structures of the FAD cofactors and the closely interacting residues of *Ec*CPD (Protein Data Bank [PDB] ID: 1DNP) (43), *Synechocystis* DASH (PDB ID: 1NP7) (17), and *Arabidopsis thaliana* 6-4 photolyase (PDB ID: 3FY4) (44). The FAD-binding pocket consisted of five residues and was highly homologous in CPF proteins (45). In each structure, a highly conserved salt bridge is formed between an arginine and an aspartic acid (Arg344 and Asp372 in *Ec*CPD) behind the *re* face of the isoalloxazine ring of FAD. An asparagine residue (Asn378 in *Ec*CPD) interacts with N5 of FAD, which is conserved in CPD photolyases, DASH proteins, 6-4 photolyases, and type II animal CRYs but is replaced with an aspartic acid in plant CRYs and with a cysteine in type I animal CRYs. Two residues are located above the *si* face of the isoalloxazine ring (Ala377 and Gly381 in *Ec*CPD). It was reported that the equivalent residue of Gly381 (Gly389 in *Synechococcus elongatus* CPD photolyase) ensured the kinetic

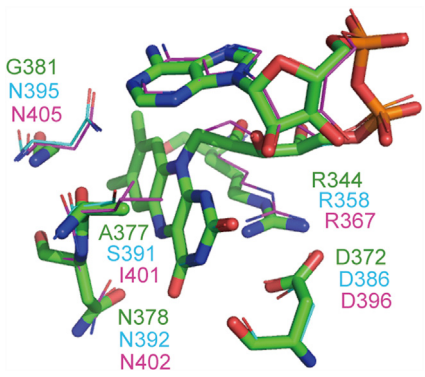

Figure 2. Structure alignment of the FAD cofactors and the closely interacting residues of three CPF proteins. The cofactor and residues of *Ec*CPD (PDB ID: 1DNP) were shown in *green stick* representations. Those of *Synechocystis* DASH (PDB ID: 1NP7) and *Arabidopsis thaliana* 6-4 photolyase (PDB ID: 3FY4) were shown in *cyan* and *magenta lines*, respectively. FAD, flavin adenine dinucleotide; PDB, Protein Data Bank.

stability of the NSQ state (19), which is replaced with an asparagine in DASH proteins, 6-4 photolyases, and type I animal CRYs and with a serine in many type II animal CRYs. Sequence alignments showed that the distribution of the residues at site 377 has an interesting pattern in the CPF proteins. About 86% of CPD I/III photolyases have residues with small or polar side chains, such as Ala, Ser, and Asn, at this site. About 90% of DASH proteins contain Ser at this site. By contrast, ∼91% of 6-4 photolyases and all animal CRYs have bulky hydrophobic residues such as Ile, Leu, and Val at this site (41). Above all, only Ala377 have greater diversity in different CPF proteins, especially between CPD photolyase and 6-4 photolyase family.

In our previous study, it was found that the presence of polar residues at site 377 increased the preferences of *Ec*CPD and *d*CRY (a type I animal CRY) for HQ, while the presence of hydrophobic residues had an adverse effect (41). In this work, we conducted an intensive investigation on the effect of site 377 on the stability of HQ in three selected photolyases: *Ec*CPD, a representative of class I/III CPD photolyases with Ala at this site; *Ma*DASH, a representative of DASH proteins with Ser (Ser386) at this site; and *Pt*CPF1, a 6-4 photolyase with Ile (Ile423) at this site. The sequence alignment of these three proteins was shown in Fig. S1.

Spectroscopy of the WT and the mutant photolyases

WT *Ec*CPD and the A377S, A377N and A377I, A377L, A377V mutants were purified with the antenna cofactor methyltetrahydrofolate (MTHF) and with most of the FAD cofactor in the NSQ state. The fresh purified A377I mutant also showed absorption peaks around 450 nm, indicating that it contained some OX state FAD. For the convenience of spectroscopic analyses, the MTHF cofactor in these proteins was removed by water washing and sodium borohydride treatment (46, 47). The absorption peak of the D_0 to D_1 transition of the NSQ in *Ec*CPD (584 nm) was blue-shifted to 582 nm in A377S and to 580 nm in A377N; conversely, in A377I, A377L, and A377V about this absorption peak was red-shifted to 588 nm, 589 nm, 587 nm, respectively (Figs. 3*A* and S2, *black lines*). Nevertheless, the absorption peak of the S_0 to S_1 transition of the OX in *Ec*CPD (443 nm) was blue-shifted to 441 nm in A377S and was red-shifted to 447 nm in A377I and A377V, and to 448 nm in A377L (Figs. 3*A* and S2, red lines).

Purified *Ma*DASH and its Ser386 mutants also contained the antenna cofactor MTHF that had strong absorption at ∼384 nm (the insets of Fig. 3*B*). The MTHF cofactor could be decomposed by photobleaching (48). However, we had found that this treatment would change the structure and the redox properties of the proteins. Therefore, these proteins were analyzed without removing the MTHF cofactor. The FAD cofactor in the fresh purified *Ma*DASH and the S386N mutant was mainly in the HQ and NSQ states, which showed that these proteins had high HQ stability against oxidation. Meanwhile, the fresh S386A and S386I, S386L, S386V mutants contained some amounts of the OX in addition to the NSQ and HQ, indicating that their HQ stability was impaired. The absorption peak of the D_0 to D_1 transition of the NSQ in *Ma*DASH was significantly red-shifted to 594 nm compared with that in *Ec*CPD (584 nm). In the S386A and S386I mutants, this absorption peak was further red-shifted to 596 nm

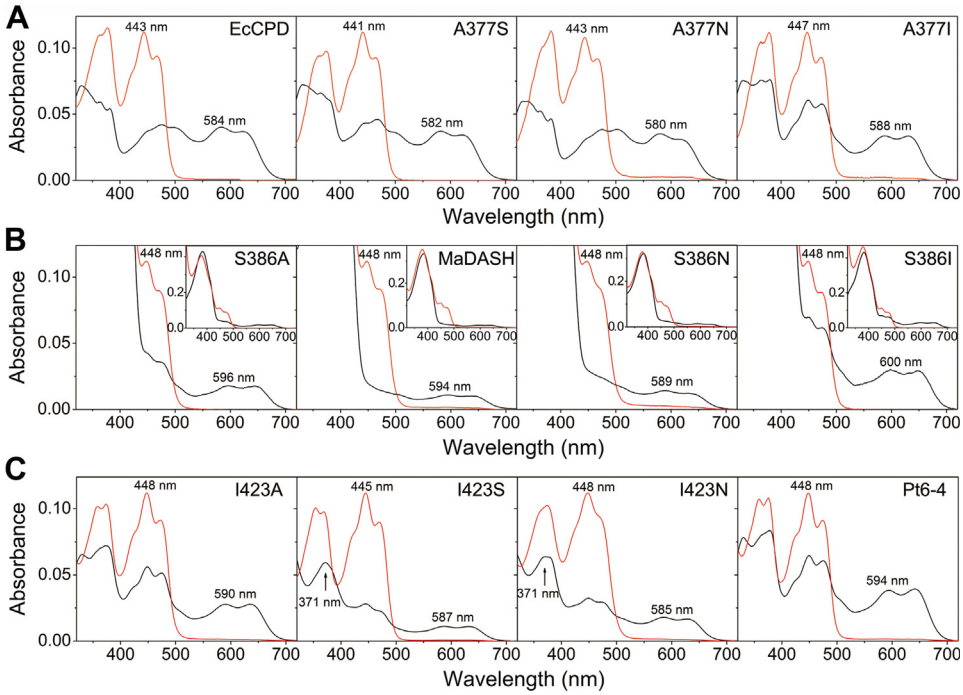

Figure 3. Absorption spectra of photolyases and their mutants. *A*, *Ec*CPD and its mutants, (*B*) *Ma*DASH and its mutants, and (*C*) *Pt*CPF1 and its mutants. The *black lines* were of fresh proteins and the *red lines* were of fully oxidized proteins. The representative absorption peaks of the HQ, SQ, and OX states FAD were indicated. All spectra were recorded with ∼10 μM of the proteins. FAD, flavin adenine dinucleotide; HQ, hydroquinone; OX, oxidized; SQ, semiquinone.

and 600 nm, respectively. In contrast, the NSQ peak in the S386N mutant was blue-shifted to 589 nm (Fig. 3*B*, *black lines*). The absorption peak of the S_0 to S_1 transition of the OX in *Ma*DASH was at 448 nm, which was barely changed in its Ser386 mutants (Fig. 3*B*, *red lines*).

*Pt*CPF1 and its I423A, I423L, and I423V mutants were isolated with the FAD cofactor in a mixture of the NSQ and OX states, without any antenna cofactor (Figs. 3*C* and S2). The spectra of the fresh purified I423S and I423N mutants showed that they had absorption peaks at ~371 nm (Fig. 3*C*, *black lines*). There was no evidence that these mutants contained an antenna cofactor because the oxidized I423S and I423N proteins showed the typical spectra of the protein-bound OX without an additional peak at ~371 nm (Fig. 3*C*, *red lines*). Nevertheless, the spectra of the "fresh" I423S and I423N proteins could be reproduced with the oxidized proteins when they were photoreduced and partially oxidized again. Therefore, the peaks at ~371 nm are indicative of the presence of HQ in the fresh I423S and I423N proteins, implying that these two mutants had significantly improved HQ stability. The absorption peak of the D_0 to D_1 transition of the NSQ in *Pt*CPF1 (594 nm) was blue-shifted in I423A (590 nm), I423S (587 nm), and I423N (585 nm) (Fig. 3*C*, *black lines*). The absorption peak of the S_0 to S_1 transition of the OX in *Pt*CPF1 (448 nm) was blue-shifted in I423S (444 nm) (Fig. 3*C*, *red lines*).

Photoreduction of the WT and the mutant photolyases

Photolyases need HQ to perform their repair functions (3–6). The FAD cofactor of photolyases in the OX or the NSQ state can be photoreduced to the HQ state in the presence of external electron donors such as DTT (49). To investigate the effect of the residues at site 377 on photoreduction, the quantum yields of photoreduction from NSQ to HQ in the WT and mutant photolyases were determined. The protein samples were supplemented with 10 mM DTT and illuminated under anaerobic conditions with a red LED lamp (λ_{max} ~632 nm), which exclusively excites the NSQ. The spectra of the samples were recorded at intervals. The fraction of the NSQ remaining at time t ($[NSQ]_t/[NSQ]_0$) was fitted with a single-exponential equation:

$$[NSQ]_t / [NSQ]_0 = e^{-k_p It} \quad (1)$$

Where k_p is the photolytic constant and I is the irradiance in W m^{-2}. The quantum yield of photoreaction (Φ) could be obtained by the equation (50):

$$\Phi = 5.2\times10^8 k_p\left(m^2J^{-1}\right)\lambda^{-1}(nm)\varepsilon^{-1}\left(M^{-1}cm\right) \quad (2)$$

Where λ is the wavelength of illumination, and ε is the molar extinction coefficient at λ.

The photolytic constants and the calculated quantum yields of photoreduction are listed in Table 1. It was found that the A377S and A377N mutants showed higher quantum yields (0.064 and 0.100) than *Ec*CPD (0.049), which was very similar to quantum yields (0.059) in early research (51). However, the quantum yield of the mutant A377I (0.011), A377L (0.006), and A377V (0.018) were dramatically impaired ($p < 0.05$). The photoreduction quantum yield of *Ma*DASH was only 0.011. The quantum yields of the S386A and S386N mutants (0.007 and 0.009) were comparable to *Ma*DASH but that of the S386I mutant (0.004) was much lower ($p < 0.05$). Under the same conditions, *Pt*CPF1 had an obviously higher quantum yield (0.120) compared with the other photolyases. The quantum yields of I423S (0.167) and I423N (0.160) were even higher than that of *Pt*CPF1, although the significant difference was only between those of I423S and *Pt*CPF1 ($p < 0.05$).

Table 1
Photoreduction of the wild-type and mutant photolyases from NSQ to HQ

Protein	ε_{632} (M^{-1} cm^{-1}) [a]	k_p (× 10^{-4} m^2 J^{-1}) [b]	Φ[c]
*Ec*CPD	4060	2.42 ± 0.14	0.049 ± 0.003
A377S	3950	3.06 ± 0.17	0.064 ± 0.004
A377N	3170	3.84 ± 0.89	0.100 ± 0.023[d]
A377I	5390	0.71 ± 0.15	0.011 ± 0.002[d]
A377L	4251	0.31 ± 0.08	0.006 ± 0.002[d]
A377V	4040	0.90 ± 0.03	0.018 ± 0.001[d]
*Ma*DASH	4420	0.57 ± 0.07	0.011 ± 0.001
S386A	4720	0.43 ± 0.09	0.007 ± 0.002[e]
S386N	4230	0.46 ± 0.03	0.009 ± 0.001
S386I	4390	0.24 ± 0.05	0.004 ± 0.001[e]
S386L	5032	0.43 ± 0.04	0.007 ± 0.001[e]
S386V	4368	0.41 ± 0.11	0.008 ± 0.002[e]
*Pt*CPF1	5080	7.39 ± 0.66	0.120 ± 0.011
I423L	4323	6.09 ± 3.60	0.116 ± 0.068
I423V	4670	8.91 ± 0.05	0.157 ± 0.001
I423A	4820	7.39 ± 0.45	0.126 ± 0.008
I423S	3530	7.15 ± 0.16	0.167 ± 0.004[f]
I423N	3910	7.62 ± 1.27	0.160 ± 0.027

[a] ε_{632}, the molar extinction coefficient at the wavelength of illumination, 632 nm.
[b] k_p, the photolytic constant.
[c] Φ, the quantum yield of photoreduction.
[d] $p < 0.05$ *versus* *Ec*CPD.
[e] $p < 0.05$ *versus* *Ma*DASH.
[f] $p < 0.05$ *versus* *Pt*CPF1. Data are mean ± SD, n =3. Statistical analyses were one-way ANOVA, post-hoc Tukey test.

Oxidation kinetics of the WT and the mutant photolyases

To further explore the roles of site 377, the oxidation kinetics of the WT and the mutant photolyases were investigated. The protein samples were quickly photoreduced to the HQ state and were then allowed to be oxidized under aerobic conditions in the dark. The absorption spectra were recorded at intervals. The time-dependent fractions of the HQ, NSQ, and OX in each sample were calculated according to the spectra. Representative results are shown in Figures 4 and S3–S7.

The kinetics of the HQ and NSQ components were analyzed according to the following schemes (19):

$$HQ \xrightarrow{k_1} NSQ \xrightarrow{k_2} OX$$
$$HQ \xrightarrow{k_3} OX$$

Assuming each step proceeded with the irreversible first-order kinetics, the time-dependent concentrations of the HQ

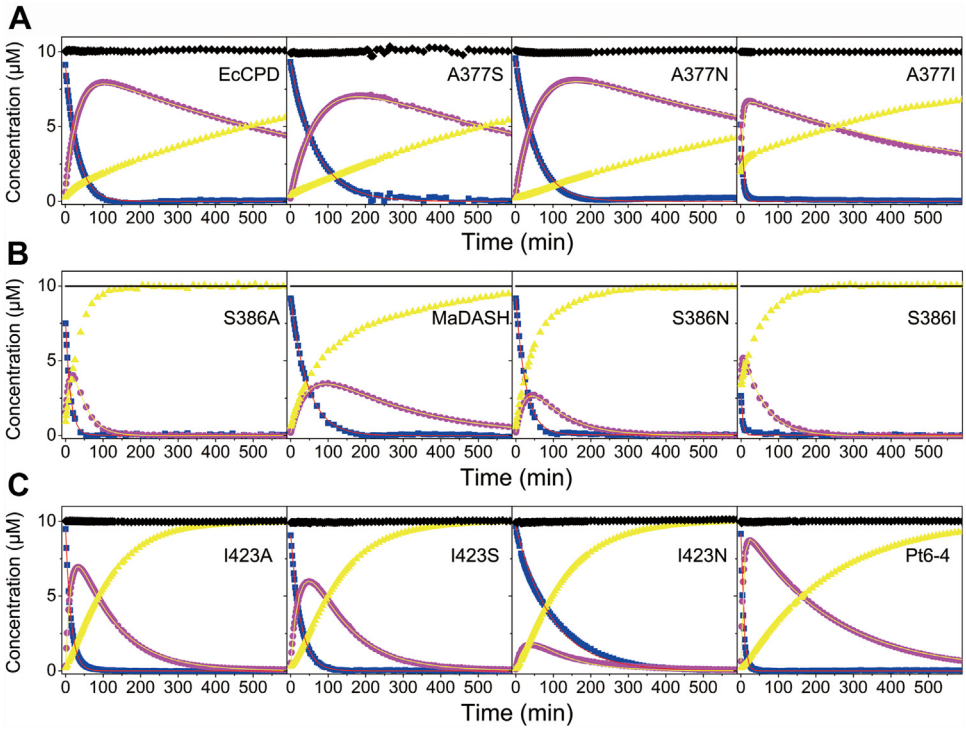

Figure 4. Oxidation kinetics of photolyases and their mutants. *A*, *Ec*CPD and its mutants, (*B*) *Ma*DASH and its mutants, and (*C*) *Pt*CPF1 and its mutants. The time-dependent concentrations of the HQ (*blue box*), NSQ (*magenta circle*), and OX (*yellow triangle*) in each sample were shown. For all samples, the total concentrations of the holo-proteins (*black diamonds* or *lines*) were of ~10 μM. Representative results of three independent experiments for each protein are shown. HQ, hydroquinone; NSQ, neutral semiquinone.

and NSQ components could be simulated by the following equations:

$$[\mathrm{HQ}]_t = [\mathrm{HQ}]_0 e^{-(k_1+k_3)t} \quad (3)$$

$$[\mathrm{NSQ}]_t = [\mathrm{HQ}]_0 \frac{k_1}{k_2-(k_1+k_3)}\left[e^{-(k_1+k_3)t} - e^{-k_2 t}\right] + [\mathrm{NSQ}]_0 e^{-k_2 t} \quad (4)$$

Where the indices 0 and t specify the concentrations of the HQ and NSQ at t = 0 and t. The item $[\mathrm{NSQ}]_0$ was added to address any NSQ component that was not reduced at t = 0.

The fitting results are shown in Table 2. Among three WT photolyases, *Pt*CPF1 had the highest oxidation rate of HQ ($k_1 + k_3 = 24.22 \times 10^{-4}$ s^{-1}). This was in accordance with the observations that many 6-4 photolyases were oxidized much faster than CPD photolyases during purification (52–56). The results also revealed that substituting different types of the residues at site 377 in these proteins affected the stability of HQ toward oxidation in different manners. Among each WT photolyase and their respective mutants, the proteins containing the hydrophobic residue Ile, Leu, and Val at site 377 (in *Ec*CPD, *Ma*DASH, and WT *Pt*CPF1) had the highest oxidation rates of HQ. Meanwhile, the proteins containing polar residues such as Ser or Asn at this site always had the lower oxidation rates of HQ. The oxidation rates of the HQ in the proteins containing Ala at this site were at intermediate levels among these proteins.

For *Ec*CPD and *Pt*CPF1 and their mutants (except for A377I, A377L, and A377V), their rate constants of direct oxidation from HQ to OX (k_3) were negligible, which revealed that HQ in these proteins was oxidized in a sequential manner. However, direct oxidation from HQ to OX contributed a significant part of the HQ oxidation in *Ma*DASH and its mutants. The effect of residue substituting at site 377 on the oxidation rates of NSQ (k_2) in these proteins was obscure. The A377N mutant had a lower oxidation rate of NSQ compared to its WT. But in most of the other mutants, the k_2 values were largely elevated. It might be due to that the stability of NSQ was very sensitive to the subtle changes in the structures of the mutants.

Repair activity of the WT and the mutant photolyases in vitro

The effect of residue substituting at site 377 on the repair activity of the photolyases *in vitro* was investigated. The results were shown in Table 3 and Figs. S8, S9. For three kinds of photolyase, a longer initial lag phase was observed in mutants with Ile, Leu, and Val residues. Interestingly, WT photolyase and its mutants had significant differences on repair rates and quantum yields for CPD lesions in DNA. In *Ec*CPD and *Ma*DASH photolyase, the repair activity of mutant with hydrophilic residues was higher than that with hydrophobic amino acids, and the apparent quantum yield was much more than that of the latter. The repair function of mutant A377S and A377N were enhanced but A377I, A377L, and A377V had the exactly opposite effect. Moreover, the repair rates of the S386I mutants were obviously lower than that of *Ma*DASH

Table 2
The oxidation kinetics of the WT and mutant photolyases

Protein	$k_1 + k_3$ ($\times 10^{-4}$ s^{-1})	k_1 ($\times 10^{-4}$ s^{-1})	k_3 ($\times 10^{-4}$ s^{-1})	k_2 ($\times 10^{-5}$ s^{-1})
*Ec*CPD	4.94 ± 0.74	4.65 ± 0.51	0.29	2.16 ± 0.08
A377S	2.70 ± 0.34	2.60 ± 0.30[a]	0.10	2.67 ± 0.76
A377N	3.53 ± 0.46	3.43 ± 0.57	0.10	1.56 ± 0.03
A377I	28.31 ± 2.05[a]	21.50 ± 0.76[a]	6.81	4.39 ± 2.69
A377L	24.00 ± 4.04[a]	14.30 ± 5.62[a]	9.67	1.42 ± 0.29
A377V	15.80 ± 0.28[a]	6.00 ± 0.01	8.38	5.18 ± 0.04
*Ma*DASH	4.19 ± 0.93	2.24 ± 0.94	1.95	6.82 ± 0.33
S386A	12.40 ± 1.70[b]	10.80 ± 1.08[b]	1.60	51.02 ± 3.60[b]
S386N	6.30 ± 0.14	2.60 ± 0.42	3.70	18.78 ± 1.54[b]
S386I	30.13 ± 4.29[b]	26.22 ± 5.42[b]	3.91	30.31 ± 0.28[b]
S386L	12.40 ± 2.19[b]	2.10 ± 0.52	10.30	4.43 ± 0.57
S386V	11.51 ± 2.32[b]	9.32 ± 1.51[b]	2.19	8.33 ± 1.72
*Pt*CPF1	24.22 ± 0.44	24.13 ± 0.65	0.09	7.43 ± 0.15
I423L	20.60 ± 2.17	18.45 ± 10.60	2.14	18.73 ± 1.59
I423V	8.63 ± 1.45[c]	9.72 ± 0.67[c]	−1.08	10.51 ± 1.72
I423A	12.20 ± 0.98[c]	11.81 ± 1.09[c]	0.39	16.03 ± 0.22
I423S	6.44 ± 0.06[c]	6.32 ± 0.97[c]	0.12	16.39 ± 0.16
I423N	1.87 ± 0.12[c.]	2.22 ± 0.21[c]	-0.35	80.51 ± 1.30[c]

[a] $p < 0.05$ *versus* *Ec*CPD.
[b] $p < 0.05$ *versus* *Ma*DASH.
[c] $p < 0.05$ *versus* *Pt*CPF1. Data are mean ± SD, n =3. Statistical analyses were one-way ANOVA, post-hoc Tukey test.

and S386N. The initial lag phase of the S386I mutant was longer and the repair activity was dramatically impaired. It was found the quantum yield of *Ma*DASH (0.111, with the MTHF cofactor) for CPDs in oligonucleotide was lower than that of *Ec*CPD (0.503, without MTHF, which was similar to that of 0.626 reported by Payne G & Sancar A (57)). In addition, *Pt*CPF1 and its mutants had similar rates and quantum yields during repairing 6-4 photoproducts in DNA, but the initial lag phases of *Pt*CPF1 and I423A were longer compared to those of I423S and I423N.

Repair activity of the WT and the mutant photolyases in vivo

To verify whether the residues at site 377 affect the photorepair activity *in vivo*, the genome of *E. coli* MG1655 was edited using the CRISPR-Cas9 system to express A377S, A377N, and A377I and KO Δ*phr* mutant of *Ec*CPD. The WT and the mutant strains were irradiated with UVC and then illuminated under 380 nm UVA light to conduct photorepair. The repair kinetics were analyzed through the survival rate in unit time, which was calculated by the ratio of initial UVC-untreated CFUs (CFU_0) and UVC-treated CFUs. As shown in Table 4, Figs. 5 and S10, the photorepair activity in the mutant strains was comparable to that in the WT MG1655 strain. Due to having no photolyase gene, the survival rate of Δ*phr* mutant kept much lower level than other strains. And, compared to *E. coli* MG1655, the photorepair activity of A377S and A377N remained almost the same but that of A377I performed obviously a lower level, which was nearly consistent with repair activity of the WT and the mutant photolyases *in vitro*. It was shown that the hydrophilic amino acids at 377 site indeed had enhanced effect on the photorepair activity of CPD photolyase but hydrophobic residues play an impaired role of repair rate of CPD photolyase *in vivo*.

Table 3
Photorepair activity of the WT and mutant photolyases *in vitro*

Protein	ε_{380} (M^{-1} cm^{-1}) [a]	*lag* (s) [b]	k_p ($\times 10^{-3}$ m^2 J^{-1}) [c]	Φ[d]
*Ec*CPD[e]	4444	63.41 ± 20.41	1.59 ± 0.13	0.503 ± 0.041
A377S[e]	4213	51.97 ± 8.10	1.58 ± 0.16	0.527 ± 0.053
A377N[e]	4113	25.95 ± 9.30[f]	1.75 ± 0.02	0.598 ± 0.007[f]
A377I[e]	5349	248.92 ± 32.30[f]	0.65 ± 0.08[f]	0.171 ± 0.021[f]
A377L[e]	4831	216.67 ±16.02[f]	1.27 ± 0.10	0.369 ± 0.029[f]
A377V[e]	4844	399.87 ± 63.80[f]	0.46 ± 0.09[f]	0.133 ± 0.026[f]
*Ma*DASH	39,300	−2.49 ± 2.01	3.16 ± 0.09	0.111 ± 0.032
S386A	41,000	1.98 ± 4.31	1.28 ± 0.04[g]	0.043 ± 0.012[g]
S386N	38,200	−3.84 ± 0.45	1.78 ± 0.03[g]	0.064 ± 0.010[g]
S386I	40,400	90.41 ± 31.12[g]	0.08 ± 0.01[g]	0.029 ± 0.004[g]
*Pt*CPF1	5690	12.80 ± 3.21	0.26 ± 0.03	0.064 ± 0.007
I423A	5520	23.95 ± 4.97[h]	0.27 ± 0.01	0.074 ± 0.001
I423S	5500	4.42 ± 0.69[h]	0.30 ± 0.02	0.068 ± 0.003
I423N	5300	2.95 ± 0.32[h]	0.27 ± 0.02	0.068 ± 0.004

[a] ε_{380}, the molar extinction coefficient at the wavelength of illumination, 380 nm.
[b] The initial lag phase time was estimated as the abscissa-intercept of the fitted line.
[c] k_p, the photolytic constant.
[d] Φ, the quantum yield of photorepair.
[e] The MTHF cofactor was removed.
[f] $p < 0.05$ *versus* *Ec*CPD.
[g] $p < 0.05$ *versus* *Ma*DASH.
[h] $p < 0.05$ *versus* *Pt*CPF1. Data are mean ± SD, n =3. Statistical analyses were one-way ANOVA, post-hoc Tukey test.

Table 4
Photorepair activity of the WT and mutant photolyases *in vivo*

Protein	*E.coli* MG1655	A377S	A377N	A377I	Δ*phr*
Activity ($\times 10^{-2}$ sec^{-1})	0.336 ± 0.041	0.345 ± 0.004	0.322 ± 0.009	0.226 ± 0.070[a]	0.063 ± 0.007[a]

[a] $p < 0.05$ *versus E. coli* MG1655.

Discussion

In this study, we investigated three representative photolyases (*Ec*CPD, *Ma*DASH, and *Pt*CPF1) and the roles of different residues at site 377. It was found that in *Pt*CPF1, which contained a hydrophobic residue Ile at site 377, the HQ FAD oxidized much faster than that in the other two ones. Nevertheless, the mutants containing polar residues such as Ser or Asn generally had higher photoreduction quantum yields and lower oxidation rates of HQ compared with their respective WT, and for the mutants containing the hydrophobic residue Ile at site 377, the opposite was always true. Most importantly, it was shown that the hydrophilic amino acids at 377 site enhanced the photorepair activity of CPD photolyase but hydrophobic residues play an opposite role of repair rate *in vitro* and *in vivo*. These results demonstrated that the residues at site 377 could turn the stability of HQ. As previously reported, 377 site of most photolyases were preferred to choose Ala, Asn, and Ser residues but the frequency of Ile, Leu, and Val were at a low level under natural conditions (41). Why 377 site have a preference for hydrophilic amino acids in photolyase? What is the mechanism of HQ stability? We speculated that there is an interaction between 377 site and pyrimidine ring of FAD. Because of N atom of pyrimidine containing a certain extent polarity, $FADH^-$ with negative charge could attract to hydrophilic residues and stabilize construction FAD-binding pocket. Adversely, hydrophobic amino acids would have a repulsive interaction to $FADH^-$ pyrimidine so that decline affinity of fully reduced FAD cofactor and protein. The stable $FADH^-$ is crucial to repair DNA lesions for photolyase, which perhaps explains why polar residues always occur in 377 site. Just as the photorepair experiment showed that the activity of *Ec*CPD photolyase with Ala, Asn, and Ser at 377 site were obvious superior to these protein with hydrophobic residues *in vitro* or *in vivo*.

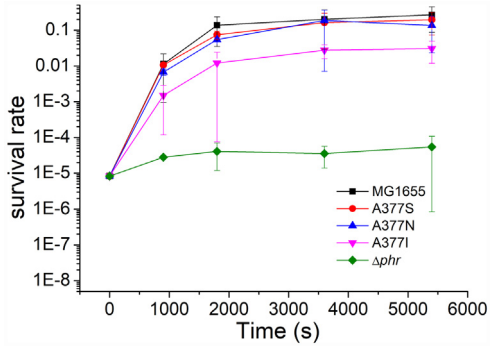

Figure 5. The photorepair kinetics of *in vivo* photorepair kinetics of *E. coli* MG1655 (■) and A377S (●), A377N (▲), A377I (▼), Δ*phr* (◆). The survival was plotted *versus* the illuminating time. Each point represents three data measurements, and the bars represent the SDs.

Both CPD and 6-4 photolyases require the HQ FAD for catalysis (3–6). Therefore, the stable HQ state would be of benefit in maintaining the activity of photolyases. Indeed, most CPD photolyases (including DASH proteins) have the residues with small or polar side chains (Ala, Ser, and Asn) at site 377. However, most of 6-4 photolyases, including *Pt*CPF1, contained hydrophobic residues at site 377, which would destabilize the HQ state. Actually, although the WT *Pt*CPF1 and its mutants at site 377 had similar repair rates and quantum yields, the initial lag phase of the WT was a bit longer than those of the mutants containing Ser or Asn at site 377. It was also found that the mutants of *Ec*CPD and *Ma*DASH containing Ile, Leu, and Val at site 377 had longer initial lag phases. The physiological significance of the presence of hydrophobic residues at site 377 in most of 6-4 photolyases remains unclear. Perhaps it might be beneficial to the primitive CRY activity of some 6-4 photolyases (27–30).

As most 6-4 photolyases, animal CRYs also contain hydrophobic residues at site 377. It was showed that WT *d*CRY could only be photoreduced to the ASQ state. But its V415S and V415N mutants (Val415 is the equivalent residue at site 377) could be further photoreduced to the HQ state, indicating the stability of the HQ was increased in these mutants (41). Therefore, the roles of the residues at site 377 on the stability of HQ might be universal throughout the CPF proteins. The occurrence of hydrophobic residues at site 377 should be an important event during the evolution of animal CRYs from photolyases, which might help animal CRYs to utilize the SQ state as their possible signaling states.

A common effect of residue substituting at site 377 was on the spectra of the proteins. Replacement of the residue at site 377 with the hydrophobic residue Ile generally led to a red-shift of the absorption peaks of FAD. Meanwhile, in the mutants containing the polar residues such as Ser or Asn, the peaks of FAD were blue-shifted. We speculated that the hydrophobic residue at site 377 might disperse the electron in the isoalloxazine ring of FAD, causing more extended delocalization of the π-electron system. The repulsive force between the hydrophobic residue and the polar isoalloxazine ring might also destabilize the electron-rich HQ state. In contrast, the polar residue at site 377 might attract the electron in the isoalloxazine ring, causing less extended delocalization of the π-electron system, and stabilize the HQ state.

It is interesting that although *Pt*CPF1 has a lower HQ stability, it has a higher photoreduction quantum yield compared to the other photolyases. It seems that *Pt*CPF1 has gained improved photoreduction ability during evolution to compensate its lower HQ stability. It was also found that *d*CRY and other type I animal CRYs have high photoreduction quantum yields (37), which may contribute to their highly photosensitivity. It was found that 6-4 photolyases contain

some distinct structural features, such as the phosphate-binding motif, the Pro-Lys-Leu protrusion motif, and the sulfur loop, which also found in animal CRYs (7). The sulfur loop is located near the external end of the Trp electron transfer chain for photoreduction. The electron-rich sulfur residues in the sulfur loop (such as Met318 and Cys324 in *A. thaliana* 6-4 photolyase, Met331 and Cys337 in *d*CRY) may facilitate the photoreduction of 6-4 photolyases and animal CRYs (7). In PtCPF1, the corresponding residues are Met340 and Ala346; the former may act as the electron donor. Nevertheless, besides the classic Trp triad that is conserved in many photolyases and CRYs, a fourth electron-transferring Trp was exclusively found in 6-4 photolyases and animal CRYs, including PtCPF1 and *Drosophila* CRY (58). The fourth electron-transferring Trp might also increase the photoreduction efficiency of 6-4 photolyases and animal CRYs.

The phosphate-binding and Pro-Lys-Leu protrusion motifs of 6-4 photolyases constrict the entrance to the substrate-binding cavity above the FAD cofactor (7). These structures may help 6-4 photolyases hold FAD tightly even in the unstable HQ state. During the repair reaction of the 6-4 photoproduct, there is a transient water molecule or a hydroxyl group to be transferred to the 3′ base (59, 60). The constricted binding cavity may be crucial for the catalysis. In FeS-BCP proteins, a long linker after helix-α7 that wraps around the active site may perform a similar function (61, 62). Therefore, the failure to convert a CPD photolyase to a 6-4 photolyase (8) may be due to the absence of these structural features in CPD photolyases.

It was observed that the NSQ oxidation rates of *Ma*DASH and *Pt*CPF1 were faster than that of *Ec*CPD. This difference might not be attributed to the residues at site 377 because the mutants of this site had different effects on the oxidation rates of NSQ. Other structural differences might be responsible for the changes of the oxidation rates of NSQ. One candidate is site 381 (Gly381 in *Ec*CPD, Asn390 in *Ma*DASH, and Asn427 in *Pt*CPF1), which was proved to affect the kinetic stability of the NSQ state (19). During the evolution route from photolyases to animal CRYs, these changes might have happened: class I/III CPD photolyases (with highly stable HQ state, highly stable NSQ state) → DASH proteins (with highly stable HQ state, low stable NSQ state) → 6-4 photolyases (with low stable HQ state, low stable NSQ state) → animal CRYs (with no stable HQ state, low stable SQ state). The faster oxidation rates of SQ enable CRYs to recover to the OX state quickly in dark. Further investigation on key residues that are different in photolyases and CRYs may shed new light on the evolutionary route between them.

Experimental procedures

Sequence analyses

Sequences of the CPF proteins were retrieved from the National Center for Biotechnology Information (NCBI, http://www.ncbi.nlm.nih.gov). Multiple sequence alignments were performed using Clustal W with Identity protein weight matrix (63). Phylogenetic analyses and tree constructions were performed using MEGA 7.0 (http://www.megasoftware.net) with the maximum likelihood function (64). The final phylogenetic tree was constructed with 37 selected sequences. The reliability of the final tree was evaluated using 500 bootstrap iterations.

Cloning, mutagenesis, expression, and purification

The plasmid phr(N + X) harboring the *E. coli phr* gene was used to overexpress *Ec*CPD (46). The algae strains *M. aeruginosa* and *P. tricornutum* were purchased from the Freshwater Algae Culture Collection at the Institute of Hydrobiology. The *M. aeruginosa DASH* gene was obtained by PCR with genomic DNA of *M. aeruginosa* as the template. The *P. tricornutum* 6-4 photolyase gene (*PtCPF1*) was obtained by RT-PCR with total RNA of *P. tricornutum* as the template. The two genes were cloned into pET22b, to obtain the plasmid pMAdash and pPT64, respectively. Site-directed PCR mutagenesis was used to generate the mutants of *Ec*CPD (A377S, A377N, A377I, A377V, and A377L), of *Ma*DASH (S386A, S386N, S386I, S386V, and S386L), and of *Pt*CPF1 (I423A, I423S, I423N, I423V, and I423L). The recombinant plasmids were transformed into competent BL21(DE3) or Rosetta(DE3) cells (Novagen). The cells were grown at 37 °C in LB medium containing 100 μg ml^{-1} ampicillin. When A_{600} reached 0.8 to 1.0, protein expression was induced with 1 mM IPTG. The cells were further incubated overnight at 20 °C and then harvested and disrupted by sonication in lysis buffer (50 mM Tris–HCl, pH 7.2, 100 mM NaCl, and 10% glycerol). The proteins were purified using Ni^{2+}-chelating sepharose (GE Healthcare) and size-exclusion chromatography on a Superdex 200 10/300 GL column (GE Healthcare). For *Ec*CPD and its mutants, the MTHF cofactor could be removed by washing with deionized water (46) and then with 20 mM sodium borohydride (47) during the first purification step. The purified proteins were stored in protein buffer containing 50 mM Tris–HCl, pH 7.2, 200 mM NaCl, 1 mM EDTA, and 10% glycerol.

UV-visible spectroscopy

UV-visible spectra from 750 to 200 nm were recorded on a UV-1800 spectrophotometer with a temperature controller (Shimadzu). During spectrum recording, the protein sample was injected into a semimicro quartz cuvette of 800 μl, and the temperature was held at 18 °C. The molar extinction coefficients of the different redox states of the flavin cofactor in the proteins were calculated using the spectra taken before and after boiling and using the extinction coefficient of released free FAD_{ox} (ε_{450} = 11,300 μM^{-1} cm^{-1}).

Quantitative analyses of photoreduction

The photoreduction processes from NSQ to HQ in various protein samples were monitored. The fresh samples were used that were partially in the NSQ state. Before photoreduction, 10 mM DTT was added to the protein samples. The samples were then bubbled with argon for 10 min and sealed with paraffin oil. A red LED (λ_{max} ~632 nm) was used as the light source. Its irradiance was determined by a spectral irradiance colorimeter (OHSP-350, Hopoocolor). The absorption spectra

were monitored at intervals by which the quantum yields of the photoreaction were calculated.

Quantitative analyses of oxidation

Each protein sample was quickly photoreduced in the presence of 10 mM DTT under a mixture of blue and red light (446 nm and 632 nm) in an ice-water bath. The photoreduced sample was put into the UV-1800 spectrophotometer with a temperature-controlled cell holder and oxidized under aerobic conditions. The temperature was set at 18 ± 0.5 °C. The absorption spectra were automatically recorded at intervals. For *Ec*CPD, *Pt*CPF1, and their mutants, the HQ, NSQ, and OX components at each interval were quantified from the spectrum by multiple linear regression using the molar extinction coefficient spectra of those components as the independent data (53). For *Ma*DASH and their mutants, this approach was not feasible because of the absorption of the antenna cofactors in these proteins hampered us to obtain the molar extinction coefficient spectra of their FAD components accurately. Instead, the time-dependent changes of the absorption peaks at ∼580 to 600 nm in these proteins were used to calculate the kinetics of NSQ. And the time-dependent changes of the isobestic points of the NSQ and the OX at ∼485 to 495 nm in these proteins were used to infer the kinetics of the HQ.

Activity assays in vitro

The activity of *Ec*CPD, *Ma*DASH, *Pt*CPF1, and their mutants was measured using the methods adapted from a previous study (41). Oligo-thymidylate (oligo(dT)$_{16}$) was dissolved in water and irradiated with 254 nm UVC light to form ∼3.5 dimers (containing both CPDs and 6-4 photoproducts) per molecule. The MTHF cofactor of *Ec*CPD and its mutants was removed prior to the assays. For *Ec*CPD, *Ma*DASH, and their mutants, the activity was assayed in a 600 μl system with 0.1 μM of each protein, 10 μM UV-oligo(dT)$_{16}$, and 1 mM DTT in the protein buffer. For *Pt*CPF1 and their mutants, the assay system contained 0.5 μM of each protein, 10 μM UV-oligo(dT)$_{16}$, and 1 mM DTT. The samples were illuminated with a UVA LED (λ_{max} ∼380 nm, irradiance of ∼150 W m^{-2}). Absorption changes at 265 nm and 325 nm were recorded to determine the activities of the CPD and 6-4 photolyases, respectively.

Genome editing to make mutations of E. coli *CPD photolyase*

The pTargetF and pCas9 plasmids (Genscript) were used to edit the genome of the *E. coli* MG1655 strain (65). To lower the risk of repeated cutting the target sequence by single guide RNA (sgRNA)–Cas9 complex during making point mutations, a two-round genome editing protocol was used (66). Two sets of plasmids derived from pTargetF were constructed. The first set of plasmid pTargetF-*phr* expresses sgRNA with the original 20 bp protospacer (N_{20}) sequence of the *E. coli phr* gene (GGTGATTTGGCAGCCAATAA) before a protospacer adjacent motif. Plasmid pTargetF-*phr* also provides a donor DNA containing the upstream and downstream sequences of the original N_{20} sequence of the *E. coli phr* gene and an inserted new N_{20} sequence CAGCTCTCGGCACTGTAATC between them. The new N_{20} sequence was the artificial sequence as a protospacer of second round editing that had no chance to match anywhere in the original *E. coli* genome. The second set of plasmids pTargetF-A377S, pTargetF-A377N, and pTargetF-A377I express sgRNA with the new N_{20} sequence and provide donor DNA sequences of the corresponding mutant photolyases, respectively. To edit the genome, *E. coli* cells were electrotransformed with plasmid pCas9 and grown at 30 °C in LB with 50 μg ml^{-1}kanamycin. Arabinose of 10 mM was added to the culture when the A_{600} reached 0.1 to induce the λ-Red recombinases, which could to improve the recombination efficiency. In the first round, plasmid pTargetF-*phr* was electrotransformed and spread onto a LB plate containing 50 μg ml^{-1} kanamycin and 50 μg ml^{-1} spectinomycin. After incubation at 30 °C overnight, transformants were picked and verified whether the original N_{20} sequence had been replaced by the new N_{20} sequence in the *E. coli* genome. To cure plasmid pTargetF-*phr*, the correct colonies was cultured at 30 °C in LB with 50 μg ml^{-1} kanamycin and 0.5 mM IPTG. The second round editing was performed using plasmids pTargetF-A377S, pTargetF-A377N, and pTargetF-A377I to obtain the A377S, A377N, and A377I mutant strains, respectively. To cure plasmid pCas9, cells was cultured at 43 °C overnight in LB.

Determination of photolyase activity in vivo

The photolyase activity of the WT *E. coli* MG1655 and the A377S, A377N, and A377I mutant strains was investigated using a method adapted from previous work (67). These strains were cultured at 37 °C to stationary phase (A_{600} ∼ 3.0). The cells were harvested, washed, and diluted to a proper scale with saline solution. The cell suspensions were irradiated by 254 nm UVC light to give a dose ∼80 J m^{-2}. Then, the samples were illuminated under a 380 nm UVA LED (λ_{max} ∼380 nm, irradiance of ∼150 W m^{-2}) up to 90 min. At regular intervals, aliquots of the illuminated samples were withdrawn and spread onto LB plates. The activity of WT photolyase and the mutants *in vivo* was calculated according to the survival rates before and after illumination.

Data availability

All data are contained within the article. Sequences of the CPF proteins are available at the National Center for Biotechnology Information (NCBI, http://www.ncbi.nlm.nih.gov). The protein structures used in this study are available at the Protein Data Bank (https://www.rcsb.org/). The multiple sequence aligner CLUSTAL W is available at http://www.clustal.org/. Phylogenetic analyses and tree constructions are available at MEGA 11 (https://www.megasoftware.net/) with the maximum likelihood function. The PyMol molecular visualization suite is available at https://pymol.org/.

Supporting information—This article contains supporting information.

Acknowledgment—This work was supported by the National Natural Science Foundation of China (32071270, 31971199), the Major Science and Technology Projects in Anhui Province (202003a06020009), the Key Laboratory of Biomedicine in Gene Diseases and Health of Anhui Higher Education Institutes, and Anhui Provincial Key Laboratory of the Conservation and Exploitation of Biological Resources.

Author contributions—L. X. and G. Z. conceptualization; Y. T., M. G., and L. L. formal analysis; B. W., L. X., Y. T., and L. L. investigation; G. Z. resources; B. W., L. X., Z. J., and L. L. data curation; B. W. writing–original draft; B. W. and G. Z. writing–review & editing; G. Z. project administration; G. Z. funding acquisition.

Conflict of interest—The authors declare that they have no conflicts of interest with the contents of this article.

Abbreviations—The abbreviations used are: ASQ, anionic SQ; CRY, cryptochrome; CPD, cyclobutane pyrimidine dimer; FAD, flavin adenine dinucleotide; HQ, hydroquinone; MTHF, methyltetrahydrofolate; NSQ, neutral SQ; OX, oxidized; PDB, Protein Data Bank; sgRNA, single guide RNA; SQ, semiquinone.

References

1. Vechtomova, Y. L., Telegina, T. A., and Kritsky, M. S. (2020) Evolution of proteins of the DNA photolyase/cryptochrome family. *Biochemistry (Mosc.)* **85**, S131–S153
2. Chaves, I., Pokorny, R., Byrdin, M., Hoang, N., Ritz, T., Brettel, K., *et al.* (2011) The cryptochromes: blue light photoreceptors in plants and animals. *Annu. Rev. Plant Biol.* **62**, 335–364
3. Sancar, A. (2003) Structure and function of DNA photolyase and cryptochrome blue-light photoreceptors. *Chem. Rev.* **103**, 2203–2237
4. Liu, Z., Wang, L., and Zhong, D. (2015) Dynamics and mechanisms of DNA repair by photolyase. *Phys. Chem. Chem. Phys.* **17**, 11933–11949
5. Yamamoto, J., Martin, R., Iwai, S., Plaza, P., and Brettel, K. (2013) Repair of the (6-4) photoproduct by DNA photolyase requires two photons. *Angew. Chem. Int. Ed. Engl.* **52**, 7432–7436
6. Li, J., Liu, Z., Tan, C., Guo, X., Wang, L., Sancar, A., *et al.* (2010) Dynamics and mechanism of repair of ultraviolet-induced (6-4) photoproduct by photolyase. *Nature* **466**, 887–890
7. Hitomi, K., DiTacchio, L., Arvai, A. S., Yamamoto, J., Kim, S. T., Todo, T., *et al.* (2009) Functional motifs in the (6-4) photolyase crystal structure make a comparative framework for DNA repair photolyases and clock cryptochromes. *Proc. Natl. Acad. Sci. U. S. A.* **106**, 6962–6967
8. Yamada, D., Dokainish, H. M., Iwata, T., Yamamoto, J., Ishikawa, T., Todo, T., *et al.* (2016) Functional conversion of CPD and (6-4) photolyases by mutation. *Biochemistry* **55**, 4173–4183
9. Xu, L., Chen, S., Wen, B., Shi, H., Chi, C., Liu, C., *et al.* (2021) Identification of a novel class of photolyases as possible ancestors of their family. *Mol. Biol. Evol.* **38**, 4505–4519
10. Wang, Q., and Lin, C. (2020) Mechanisms of cryptochrome-mediated photoresponses in plants. *Annu. Rev. Plant Biol.* **71**, 103–129
11. Rivera, A. S., Ozturk, N., Fahey, B., Plachetzki, D. C., Degnan, B. M., Sancar, A., *et al.* (2012) Blue-light-receptive cryptochrome is expressed in a sponge eye lacking neurons and opsin. *J. Exp. Biol.* **215**, 1278–1286
12. Ozturk, N. (2017) Phylogenetic and functional classification of the photolyase/cryptochrome family. *Photochem. Photobiol.* **93**, 104–111
13. Zoltowski, B. D., Chelliah, Y., Wickramaratne, A., Jarocha, L., Karki, N., Xu, W., *et al.* (2019) Chemical and structural analysis of a photoactive vertebrate cryptochrome from pigeon. *Proc. Natl. Acad. Sci. U. S. A.* **116**, 19449–19457
14. Xu, J., Jarocha, L. E., Zollitsch, T., Konowalczyk, M., Henbest, K. B., Richert, S., *et al.* (2021) Magnetic sensitivity of cryptochrome 4 from a migratory songbird. *Nature* **594**, 535–540
15. Cashmore, A. R., Jarillo, J. A., Wu, Y. J., and Liu, D. (1999) Cryptochromes: blue light receptors for plants and animals. *Science* **284**, 760–765
16. Wang, Y., Veglia, G., Zhong, D., and Gao, J. (2021) Activation mechanism of *Drosophila* cryptochrome through an allosteric switch. *Sci. Adv.* **7**, eabg3815
17. Brudler, R., Hitomi, K., Daiyasu, H., Toh, H., Kucho, K., Ishiura, M., *et al.* (2003) Identification of a new cryptochrome class. Structure, function, and evolution. *Mol. Cell* **11**, 59–67
18. Song, S. H., Dick, B., Penzkofer, A., Pokorny, R., Batschauer, A., and Essen, L. O. (2006) Absorption and fluorescence spectroscopic characterization of cryptochrome 3 from *Arabidopsis thaliana*. *J. Photochem. Photobiol. B* **85**, 1–16
19. Damiani, M. J., Yalloway, G. N., Lu, J., McLeod, N. R., and O'Neill, M. A. (2009) Kinetic stability of the flavin semiquinone in photolyase and cryptochrome-DASH. *Biochemistry* **48**, 11399–11411
20. Sokolowsky, K., Newton, M., Lucero, C., Wertheim, B., Freedman, J., Cortazar, F., *et al.* (2010) Spectroscopic and thermodynamic comparisons of *Escherichia coli* DNA photolyase and Vibrio cholerae cryptochrome 1. *J. Phys. Chem. B* **114**, 7121–7130
21. Selby, C. P., and Sancar, A. (2006) A cryptochrome/photolyase class of enzymes with single-stranded DNA-specific photolyase activity. *Proc. Natl. Acad. Sci. U. S. A.* **103**, 17696–17700
22. Pokorny, R., Klar, T., Hennecke, U., Carell, T., Batschauer, A., and Essen, L. O. (2008) Recognition and repair of UV lesions in loop structures of duplex DNA by DASH-type cryptochrome. *Proc. Natl. Acad. Sci. U. S. A.* **105**, 21023–21027
23. Tagua, V. G., Pausch, M., Eckel, M., Gutierrez, G., Miralles-Duran, A., Sanz, C., *et al.* (2015) Fungal cryptochrome with DNA repair activity reveals an early stage in cryptochrome evolution. *Proc. Natl. Acad. Sci. U. S. A.* **112**, 15130–15135
24. Navarro, E., Niemann, N., Kock, D., Dadaeva, T., Gutierrez, G., Engelsdorf, T., *et al.* (2020) The DASH-type cryptochrome from the fungus *Mucor circinelloides* is a canonical CPD-photolyase. *Curr. Biol.* **30**, 4483–4490.e4
25. Rredhi, A., Petersen, J., Schubert, M., Li, W., Oldemeyer, S., Li, W., *et al.* (2021) DASH cryptochrome 1, a UV-A receptor, balances the photosynthetic machinery of *Chlamydomonas reinhardtii*. *New Phytol.* **232**, 610–624
26. Kiontke, S., Gobel, T., Brych, A., and Batschauer, A. (2020) DASH-type cryptochromes-solved and open questions. *Biol. Chem.* **401**, 1487–1493
27. Bluhm, B. H., and Dunkle, L. D. (2008) *PHL1* of *Cercospora zeae-maydis* encodes a member of the photolyase/cryptochrome family involved in UV protection and fungal development. *Fungal Genet. Biol.* **45**, 1364–1372
28. Coesel, S., Mangogna, M., Ishikawa, T., Heijde, M., Rogato, A., Finazzi, G., *et al.* (2009) Diatom PtCPF1 is a new cryptochrome/photolyase family member with DNA repair and transcription regulation activity. *EMBO Rep.* **10**, 655–661
29. Heijde, M., Zabulon, G., Corellou, F., Ishikawa, T., Brazard, J., Usman, A., *et al.* (2010) Characterization of two members of the cryptochrome/photolyase family from *Ostreococcus tauri* provides insights into the origin and evolution of cryptochromes. *Plant Cell Environ.* **33**, 1614–1626
30. Franz, S., Ignatz, E., Wenzel, S., Zielosko, H., Putu, E., Maestre-Reyna, M., *et al.* (2018) Structure of the bifunctional cryptochrome aCRY from *Chlamydomonas reinhardtii*. *Nucl. Acids Res.* **46**, 8010–8022
31. Xu, L., Mu, W., Ding, Y., Luo, Z., Han, Q., Bi, F., *et al.* (2008) Active site of *Escherichia coli* DNA photolyase: Asn378 is crucial both for stabilizing the neutral flavin radical cofactor and for DNA repair. *Biochemistry* **47**, 8736–8743
32. Damiani, M. J., Nostedt, J. J., and O'Neill, M. A. (2011) Impact of the N5-proximal Asn on the thermodynamic and kinetic stability of the semiquinone radical in photolyase. *J. Biol. Chem.* **286**, 4382–4391
33. Paulus, B., Bajzath, C., Melin, F., Heidinger, L., Kromm, V., Herkersdorf, C., *et al.* (2015) Spectroscopic characterization of radicals and radical pairs in fruit fly cryptochrome - protonated and nonprotonated flavin radical-states. *FEBS J.* **282**, 3175–3189

34. Muller, P., Brettel, K., Grama, L., Nyitrai, M., and Lukacs, A. (2016) Photochemistry of wild-type and N378D mutant E. coli DNA photolyase with oxidized FAD cofactor studied by transient absorption spectroscopy. *Chemphyschem* **17**, 1329–1340
35. Wijaya, I. M., Domratcheva, T., Iwata, T., Getzoff, E. D., and Kandori, H. (2016) Single hydrogen bond donation from flavin N5 to proximal asparagine ensures FAD reduction in DNA photolyase. *J. Am. Chem. Soc.* **138**, 4368–4376
36. Kottke, T., Batschauer, A., Ahmad, M., and Heberle, J. (2006) Blue-light-induced changes in *Arabidopsis* cryptochrome 1 probed by FTIR difference spectroscopy. *Biochemistry* **45**, 2472–2479
37. Ozturk, N., Song, S. H., Selby, C. P., and Sancar, A. (2008) Animal type 1 cryptochromes. Analysis of the redox state of the flavin cofactor by site-directed mutagenesis. *J. Biol. Chem.* **283**, 3256–3263
38. Balland, V., Byrdin, M., Eker, A. P., Ahmad, M., and Brettel, K. (2009) What makes the difference between a cryptochrome and DNA photolyase? A spectroelectrochemical comparison of the flavin redox transitions. *J. Am. Chem. Soc.* **131**, 426–427
39. Burney, S., Wenzel, R., Kottke, T., Roussel, T., Hoang, N., Bouly, J. P., *et al.* (2012) Single amino acid substitution reveals latent photolyase activity in *Arabidopsis* cry1. *Angew. Chem. Int. Ed. Engl.* **51**, 9356–9360
40. Hense, A., Herman, E., Oldemeyer, S., and Kottke, T. (2015) Proton transfer to flavin stabilizes the signaling state of the blue light receptor plant cryptochrome. *J. Biol. Chem.* **290**, 1743–1751
41. Xu, L., Wen, B., Wang, Y., Tian, C., Wu, M., and Zhu, G. (2017) Residues at a single site differentiate animal cryptochromes from cyclobutane pyrimidine dimer photolyases by affecting the proteins' preferences for reduced FAD. *ChemBioChem* **18**, 1129–1137
42. Scheerer, P., Zhang, F., Kalms, J., von Stetten, D., Krauss, N., Oberpichler, I., *et al.* (2015) The class III cyclobutane pyrimidine dimer photolyase structure reveals a new antenna chromophore binding site and alternative photoreduction pathways. *J. Biol. Chem.* **290**, 11504–11514
43. Park, H. W., Kim, S. T., Sancar, A., and Deisenhofer, J. (1995) Crystal structure of DNA photolyase from *Escherichia coli*. *Science* **268**, 1866–1872
44. Brautigam, C. A., Smith, B. S., Ma, Z., Palnitkar, M., Tomchick, D. R., Machius, M., *et al.* (2004) Structure of the photolyase-like domain of cryptochrome 1 from *Arabidopsis thaliana*. *Proc. Natl. Acad. Sci. U. S. A.* **101**, 12142–12147
45. Müller, M., and Carell, T. (2009) Structural biology of DNA photolyases and cryptochromes. *Curr. Opin. Struct. Biol.* **19**, 277–285
46. Xu, L., Zhang, D., Mu, W., van Berkel, W. J., and Luo, Z. (2006) Reversible resolution of flavin and pterin cofactors of His-tagged *Escherichia coli* DNA photolyase. *Biochim. Biophys. Acta* **1764**, 1454–1461
47. Jorns, M. S., Wang, B., and Jordan, S. P. (1987) DNA repair catalyzed by *Escherichia coli* DNA photolyase containing only reduced flavin: Elimination of the enzyme's second chromophore by reduction with sodium borohydride. *Biochemistry* **26**, 6810–6816
48. Moldt, J., Pokorny, R., Orth, C., Linne, U., Geisselbrecht, Y., Marahiel, M. A., *et al.* (2009) Photoreduction of the folate cofactor in members of the photolyase family. *J. Biol. Chem.* **284**, 21670–21683
49. Heelis, P. F., and Sancar, A. (1986) Photochemical properties of *Escherichia coli* DNA photolyase: a flash photolysis study. *Biochemistry* **25**, 8163–8166
50. Rupert, C. S. (1962) Photoenzymatic repair of ultraviolet damage in DNA. II. Formation of an enzyme-substrate complex. *J. Gen. Physiol.* **45**, 725–741
51. Payne, G., Heelis, P. F., Rohrs, B. R., and Sancar, A. (1987) The active form of *Escherichia coli* DNA photolyase contains a fully reduced flavin and not a flavin radical, both *in vivo* and *in vitro*. *Biochemistry* **26**, 7121–7127
52. Hitomi, K., Kim, S. T., Iwai, S., Harima, N., Otoshi, E., Ikenaga, M., *et al.* (1997) Binding and catalytic properties of *Xenopus* (6-4) photolyase. *J. Biol. Chem.* **272**, 32591–32598
53. Usman, A., Brazard, J., Martin, M. M., Plaza, P., Heijde, M., Zabulon, G., *et al.* (2009) Spectroscopic characterization of a (6-4) photolyase from the green alga *Ostreococcus tauri*. *J. Photochem. Photobiol. B* **96**, 38–48
54. Schleicher, E., Hitomi, K., Kay, C. W., Getzoff, E. D., Todo, T., and Weber, S. (2007) Electron nuclear double resonance differentiates complementary roles for active site histidines in (6-4) photolyase. *J. Biol. Chem.* **282**, 4738–4747
55. Todo, T., Kim, S. T., Hitomi, K., Otoshi, E., Inui, T., Morioka, H., *et al.* (1997) Flavin adenine dinucleotide as a chromophore of the *Xenopus* (6-4)photolyase. *Nucl. Acids Res.* **25**, 764–768
56. Nakajima, S., Sugiyama, M., Iwai, S., Hitomi, K., Otoshi, E., Kim, S. T., *et al.* (1998) Cloning and characterization of a gene (UVR3) required for photorepair of 6-4 photoproducts in *Arabidopsis thaliana*. *Nucl. Acids Res.* **26**, 638–644
57. Payne, G., and Sancar, A. (1990) Absolute action spectrum of E-$FADH_2$ and E-$FADH_2$-MTHF forms of *Escherichia coli* DNA photolyase. *Biochemistry* **29**, 7715–7727
58. Muller, P., Yamamoto, J., Martin, R., Iwai, S., and Brettel, K. (2015) Discovery and functional analysis of a 4th electron-transferring tryptophan conserved exclusively in animal cryptochromes and (6-4) photolyases. *Chem. Commun. (Camb.)* **51**, 15502–15505
59. Yamamoto, J., Plaza, P., and Brettel, K. (2017) Repair of (6-4) lesions in DNA by (6-4) photolyase: 20 Years of quest for the photoreaction mechanism. *Photochem. Photobiol.* **93**, 51–66
60. Maul, M. J., Barends, T. R., Glas, A. F., Cryle, M. J., Domratcheva, T., Schneider, S., *et al.* (2008) Crystal structure and mechanism of a DNA (6-4) photolyase. *Angew. Chem. Int. Ed. Engl.* **47**, 10076–10080
61. Geisselbrecht, Y., Fruhwirth, S., Schroeder, C., Pierik, A. J., Klug, G., and Essen, L. O. (2012) CryB from *Rhodobacter sphaeroides*: a unique class of cryptochromes with new cofactors. *EMBO Rep.* **13**, 223–229
62. Zhang, F., Scheerer, P., Oberpichler, I., Lamparter, T., and Krauss, N. (2013) Crystal structure of a prokaryotic (6-4) photolyase with an Fe-S cluster and a 6,7-dimethyl-8-ribityllumazine antenna chromophore. *Proc. Natl. Acad. Sci. U. S. A.* **110**, 7217–7222
63. Thompson, J. D., Higgins, D. G., and Gibson, T. J. (1994) CLUSTAL W: improving the sensitivity of progressive multiple sequence alignment through sequence weighting, position-specific gap penalties and weight matrix choice. *Nucl. Acids Res.* **22**, 4673–4680
64. Kumar, S., Stecher, G., and Tamura, K. (2016) MEGA7: molecular evolutionary genetics analysis version 7.0 for bigger datasets. *Mol. Biol. Evol.* **33**, 1870–1874
65. Jiang, Y., Chen, B., Duan, C., Sun, B., Yang, J., and Yang, S. (2015) Multigene editing in the *Escherichia coli* genome *via* the CRISPR-Cas9 system. *Appl. Environ. Microbiol.* **81**, 2506–2514
66. Wang, X., He, J., and Le, K. (2018) Making point mutations in *Escherichia coli* BL21 genome using the CRISPR-Cas9 system. *FEMS Microbiol. Lett.* https://doi.org/10.1093/femsle/fny060
67. Xu, L., Tian, C., Lu, X., Ling, L., Lv, J., Wu, M., *et al.* (2015) Photoreactivation of *Escherichia coli* is impaired at high growth temperatures. *J. Photochem. Photobiol. B: Biol.* **147**, 37–46